Spin-orbit coupling and the singlet-triplet transition in lateral double quantum dots

L. Meza-Montes
Instituto de Física, Universidad Autónoma de Puebla, Apdo. Postal J-48, Puebla 72570, Mexico

Carlos F. Destefani
Center for Photonics Research, University of Ottawa, Ottawa, Ontario, Canada K1N 6N5

Sergio E. Ulloa
Department of Physics and Astronomy, and Nanoscale and Quantum Phenomena Institute, Ohio University, Athens, Ohio 45701, USA

(Received 24 January 2008; revised manuscript received 11 September 2008; published 7 November 2008)

We study the electronic level structure in lateral double quantum dots containing one and two electrons. The calculations consider the role of spin-orbit coupling arising from structure inversion asymmetry (Rashba) and bulk inversion asymmetry (Dresselhaus), as well as the competition with diamagnetic and Zeeman effects. Utilizing a finite element approach and full diagonalization of the Hamiltonian, we explore the spatial spin textures and their progression with magnetic field. The competition of different energy scales gives rise to interesting level anticrossings and associated spin mixtures which result in weaker effective Zeeman splitting (smaller effective g factors). The singlet-triplet transition of interest for qubit operations is shown to be strongly affected in narrow band-gap materials, which should have important consequences in phonon-assisted relaxation rates.

DOI: 10.1103/PhysRevB.78.205307 PACS number(s): 73.21.La, 71.70.Ej, 73.61.Ey, 85.75.−d

I. INTRODUCTION

The proposal to use electronic spin states in quantum dots (QD) as qubits[1] has stimulated intense experimental and theoretical work. The coupling between electronic spins in a double quantum dot (DQD) is mediated by an effective interdot exchange interaction, tuned by electrostatic gates and external fields. Spin qubit operations[2,3] were recently achieved in state-of-the-art experiments in DQDs defined on a two-dimensional electron-gas (2DEG) system. By pulsing gate potentials in the DQD structure, different singlet (S) and triplet (T) electronic configurations can be achieved, where either each dot accommodates one electron or where double occupancy is allowed into one of the dots. Such delicate control of the potential profile in a two-electron system, together with the application of magnetic fields to split the triplet components, T_+, T_-, and T_0, determines the effective exchange interaction, as well as the separation between ground and first-excited states. Controlling the system so that these low-energy excitations remain distant reduces decoherence of the chosen qubit states and enhances the reliability of the effective two-level system embodied in the $S_z=0$ subspace of the lowest S and T_0 states.

Robust spin coherence is important for reliable quantum computation. Specifically, long coherence times are required to allow sufficient qubit manipulations for error correction codes to be effective.[4] The main mechanisms for electron spin decoherence are coupling to the nuclei spin (hyperfine coupling[5,6]), and the spin relaxation[7,8] caused by spin-orbit (SO) coupling mediated by phonons.[9–13] As such, these are important obstacles to overcome in achieving successful operation of integrated quantum computing in spin-based qubit systems. In this context, a complete study of SO effects on the DQD spectra is needed, including both Rashba[14] [structure inversion asymmetry (SIA)] and Dresselhaus[15] [bulk inversion asymmetry (BIA)] contributions. Such studies have been done perturbatively,[16,17] typically in a Hund-Mulliken basis where matrix elements are analytical,[18–20] in parabolic single QDs[21] and in vertically coupled DQDs.[22] The Hund-Mulliken approach is justifiable in a strongly confining potential, where excited states are highly decoupled from the lowest levels, and the perturbative approach is reliable only for wider gap materials such as GaAs, where SO effects are weaker. In QDs made on narrow-gap materials, the SO effects are much stronger, and the complex interplay with magnetic, tunneling, and Coulomb energies results in drastic effects on the spin-relaxation rates, which are only captured by a nonperturbative approach.[11,23]

This paper presents a theoretical treatment of SO coupling in laterally coupled DQDs defined on a narrow-gap material (InSb), where the system contains two electrons, and takes into account all pertinent interaction terms. We find that the competition between SO coupling, Zeeman effect, and Coulomb exchange interaction is strongly regulated by the interdot barrier amplitudes, and as such results in subtle level mixings that may drastically change the major spin component of the state. In particular, the S-T transition that occurs at finite magnetic fields for strong interdot coupling (low barrier) is transformed into clear level repulsion with the concomitant mixing of spin states. This S-T *anticrossing* introduces an energy scale $\sim$1 meV (or a time scale of $\sim$4 ps) which determines the validity of adiabatic transitions in the S-T subspace typically considered. Similarly, in the weak interdot coupling regime (high barrier), the ground state is predominantly an S arrangement with one electron in each dot and lying very close to the corresponding T manifold. Even in this regime, the states are spin mixtures and care must be taken when executing qubit operations.

II. THEORY AND MODEL

We consider a two-electron DQD defined electrostatically on a 2DEG. The Hamiltonian is $H=H_1+H_2+(e^2/\varepsilon)/|\mathbf{r}_1$

$-\mathbf{r}_2|$, where ε is the host dielectric constant, and the one-electron terms read

$$H_i = \frac{\hbar^2}{2m^*}\mathbf{k}_i^2 + \frac{g_0\mu_B}{2}\mathbf{B}\cdot\sigma_i + V(\mathbf{r}_i) + V_{\mathrm{SO}}(\mathbf{r}_i). \quad (1)$$

In Eq. (1), the first term is the kinetic energy, where m^* is the effective electron mass, $\mathbf{k}=-i\nabla+(e/\hbar c)\mathbf{A}$, with $\mathbf{A}=B(-y,x,0)/2$ in the symmetric gauge for a magnetic field $\mathbf{B}=B(0,0,1)$ perpendicular to the 2DEG. The Zeeman coupling includes the material g factor g_0, the Bohr magneton $\mu_B=e\hbar/(2m_0c)$, and the Pauli matrices σ. The third term is the potential profile defining the DQD,[24] $V(\mathbf{r})=V_c(x,y)+V_z(z)$, where

$$V_c(x,y) = -V_r e^{-[(x-a)^2+y^2]/l_r^2} - V_l e^{-[(x+a)^2+y^2]/l_l^2} + V_b e^{-x^2/l_{bx}^2 - y^2/l_{by}^2}. \quad (2)$$

The two (right and left) dots are centered at $(x,y)=(\pm a,0)$, with separation $d=2a$, and individual potentials given by the Gaussians with V_l, V_r (l_l, l_r) parametrizing the respective potential-well depth (spatial size); the third Gaussian term controls the interdot coupling, where V_b (l_{bx}, l_{by}) determines the intensity (size) of the central potential barrier. For fixed d, distinct regimes are achieved by varying V_b: from two isolated QD atoms ($V_b \gg V_l$, V_r), to one strongly coupled QD molecule, to a large elongated single dot ($V_b \ll V_l$, V_r). As such, this geometry allows one to study the competition between SO and magnetic couplings, tunneling, and direct and exchange Coulomb interactions, all of which change with the interdot barrier. For simplicity, we focus here on a symmetric DQD ($l=r$), where the two dots are identical.

The fourth term in Eq. (1) yields the SO coupling and includes both SIA and BIA contributions, $V_{\mathrm{SO}}=V_{\mathrm{SO}}^{\mathrm{SIA}}+V_{\mathrm{SO}}^{\mathrm{BIA}}$, where $V_{\mathrm{SO}}^{\mathrm{SIA}}=\alpha\sigma\cdot(\nabla V(\mathbf{r})\times\mathbf{k})$, and $V_{\mathrm{SO}}^{\mathrm{BIA}}=\gamma\Sigma_{i=1}^{3}\sigma_i k_i(k_{i+1}^2-k_{i+2}^2)$, with coupling constants α and γ, and $i=x,\ y,\ z$ (mod 3).[23] In the assumed strong vertical confinement which is provided by $V_z(z)$, only the lowest subband is populated and the in-plane and perpendicular directions decouple. Since $\langle k_z^2\rangle=(\pi/z_0)^2$ and $\langle k_z\rangle=0$, the SIA term can be decomposed into k-linear and spin-diagonal terms as $V_{\mathrm{SO}}^{\mathrm{SIA}}=V_{\mathrm{lin}}^{\mathrm{SIA}}+V_{\mathrm{dia}}^{\mathrm{SIA}}$, where

$$V_{\mathrm{lin}}^{\mathrm{SIA}} = \alpha(-dV_z/dz)(\sigma_x k_y - \sigma_y k_x), \quad (3)$$

$$V_{\mathrm{dia}}^{\mathrm{SIA}} = \alpha\sigma_z\left[\frac{\partial V_c}{\partial x}k_y - \frac{\partial V_c}{\partial y}k_x\right]. \quad (4)$$

Similarly, the BIA term is decomposed into k-linear and k-cubic terms as $V_{\mathrm{SO}}^{\mathrm{BIA}}=V_{\mathrm{lin}}^{\mathrm{BIA}}+V_{\mathrm{cub}}^{\mathrm{BIA}}$, with

$$V_{\mathrm{lin}}^{\mathrm{BIA}} = \gamma(\pi/z_0)^2(\sigma_y k_y - \sigma_x k_x), \quad (5)$$

$$V_{\mathrm{cub}}^{\mathrm{BIA}} = \gamma(\sigma_x k_x k_y^2 - \sigma_y k_y k_x^2). \quad (6)$$

Notice that the SIA coupling is tunable by the interfacial electric field dV_z/dz, as well as the interdot potential gradients, while the BIA coupling is determined by the quantum well size z_0.

We employ a finite element approach to obtain the one-electron eigenfunctions $\{\phi_n\}$ of the effective two-dimensional (2D) Hamiltonian with no B-field or SO couplings. We then determine the eigenfunctions for the full one-electron problem, $\chi_m(x,y,\sigma_z)=\Sigma_n^N\phi_n(x,y)[a_n|\uparrow\rangle+b_n|\downarrow\rangle]$, where a_n, b_n are obtained by diagonalization of H_i; $|\uparrow\rangle,|\downarrow\rangle$ are the σ_z eigenkets; and N is the size of the basis set. The two-electron eigenstates ψ_n are antisymmetric functions built from the set $\{\chi_m\}$ as

$$\psi_n = \sum_{\rho,j,k} C_{j,k}^{n,\rho}\xi_{j,k}^{\rho}(x_1,y_1,x_2,y_2)\tau^{\rho}(\sigma_{z_1},\sigma_{z_2}), \quad (7)$$

where $C_{j,k}^{n,\rho}$ are obtained by diagonalization of the full two-electron Hamiltonian H, and $\rho=S,\ T_0,\ T_+,\ T_-$. In Eq. (7),

$$\xi_{j,k}^{\rho} = N_\rho[\chi_j(x_1,y_1)\chi_k(x_2,y_2) \pm \chi_k(x_1,y_1)\chi_j(x_2,y_2)], \quad (8)$$

with the plus (or minus) sign for $\rho=S$ (or $\rho=T_0,\ T_+,\ T_-$), and N_ρ a normalization constant. The spin eigenstates τ^ρ are the well-known S-T two-particle combinations, such as $\tau^{T_-}=|\downarrow\downarrow\rangle$ and $\tau^{T_+}=|\uparrow\uparrow\rangle$.[25]

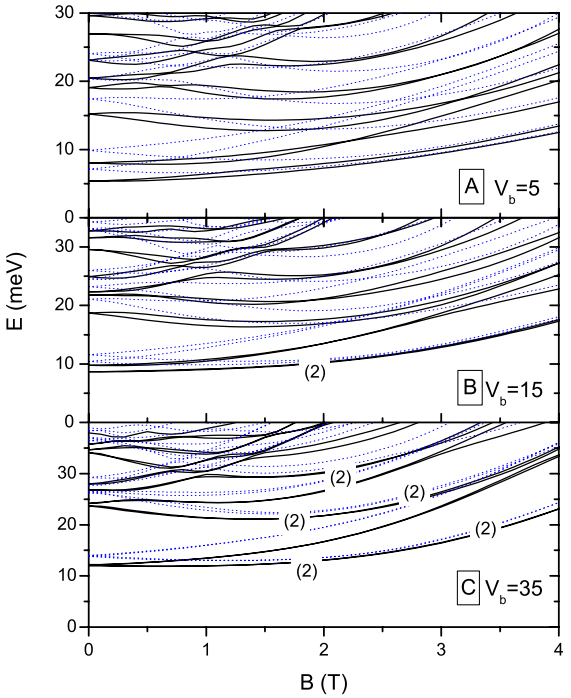

FIG. 1. (Color online) One-electron band structure as function of magnetic field. Panels A, B, and C refer, respectively, to $V_b=5$, =15, and 35 meV. Black solid (blue dashed) lines show spectrum with (without) SO coupling. The degeneracy of the lowest levels under SO coupling in shown in parenthesis.

III. ONE-ELECTRON SPECTRA

We first analyze the one-electron picture in the DQD. Figure 1 shows spectra as function of B field for different interdot coupling barriers V_b: panel A (panel C) considers a strong (weak) interdot coupling regime where $V_b=5$ (35) meV, while panel B shows an intermediate regime with $V_b=15$ meV.

In the absence of SO coupling (blue dashed lines) and in the strong interdot coupling regime (panel A), bonding

(≃7 meV at $B=0$) and antibonding (≃10 meV at $B=0$) "s"-levels (no nodes in either dot) are separated by a large effective interdot hopping integral $\delta(B=0)\simeq 3$ meV. These, as well as other higher levels, split with magnetic field, in a combination of Zeeman effect and diamagnetic shift. In panel A, at $B_{c,1e}\simeq 0.8$ T the crossing between bonding and antibonding levels occurs. For $B<B_{c,1e}$, the four lowest states have a spin sequence of ↑, ↓, ↑, ↓; for $0.8<B<1.8$ T, the spin sequence becomes ↑, ↑, ↓, ↓, and for $B>2.9$ T the lowest four levels become ↑ polarized. Level splittings and crossings involving higher excited states are also visible in the figure. At higher fields (not shown) the states collapse into highly degenerate Landau levels.[16]

As V_b increases, both $\delta(B=0)$ and $B_{c,1e}$ decrease, and the whole spectrum is shifted upward, as can be seen by comparing panels A–C. In the weak-coupling regime (panel C), the pairs of bonding and antibonding levels give way to a fourfold nearly-degenerate s-state (≃14 meV at $B=0$), as one expects for two isolated single dots.[23] Notice that the degenerate "p"-shell (with a nodal line in the spatial wave function in each dot) is not yet completely formed at $V_b=35$ meV, and some splitting is still apparent (levels at ≃27 meV at $B=0$). The lowest level crossing in panel C involves s and p orbitals at $B\simeq 3.7$ T. In other words, larger barrier results in a spectrum similar to that of an isolated QD, but with double the degeneracy for the two identical dots, as one would expect. Notice that the lowest DQD level sequence in the weak-coupling regime (panel C) is ↑, ↑ even at $B\simeq 0$, while in the strong-coupling regime such a sequence happens only when $B>B_{c,1e}$. This feature will prove to be important later for the two-electron system.

The inclusion of SO coupling in Fig. 1 (black solid lines) turns the ↑-↓ crossings into anticrossings at shifted fields, and brings the entire spectrum to lower energies, especially at low magnetic fields where SO coupling dominates magnetic terms. While the value of $\delta(B=0)$ is not much affected by SO coupling, the V_b dependence of $B_{c,1e}$, which now indicates the first *anticrossing* among s levels, is stronger [see Fig. 2(A)]. The SO coupling results also in a weaker B dependence for the spectra at low fields, especially for smaller V_b and therefore in a smaller effective g^* factor (see below).

The V_b dependence of $B_{c,1e}$ is shown in Fig. 2(A), where $B_{c,1e}$ refers to the lowest crossing (anticrossing) in the absence (presence) of SO couplings. Notice that for $V_b<10$ ($V_b>10$) meV the SO coupling shifts the critical field to larger (smaller) values when compared to the problem without SO terms. This behavior shows how the interdot barrier, and the resulting electron-tunneling energy, controls the relative importance of spin-orbit and magnetic terms in DQDs. We should note further that although the precise value of $B_{c,1e}$ would depend on confinement potential parameters, the presence of SO clearly affects this value, an effect that must be taken into consideration in experiments.

Figure 2(B) shows the effective g^* factor, scaled by g_0, as calculated from the difference in spin expectation values of the two lowest DQD levels, $g^*/g_0=\langle\Delta\sigma_z\rangle$. The smaller values ($g^*/g_0<1$) for any V_b reflect the strong spin mixing due to the SO coupling, as seen in single QDs ($g^*/g_0=1$ in the absence of SO coupling for $B\simeq 0$).[26] The g^* factor decreases rapidly with magnetic field, reflecting the near degeneracy of

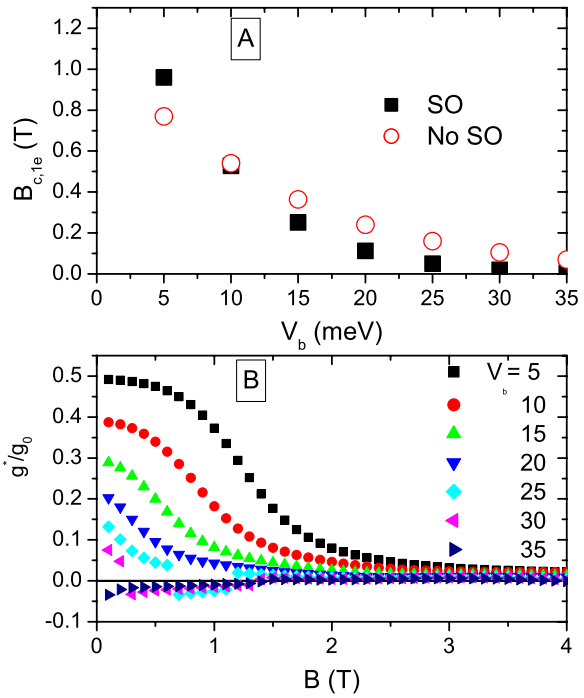

FIG. 2. (Color online) Panel A: V_b dependence of critical field $B_{c,1e}$ in the absence (crossing field, red circles) and in the presence (anticrossing field, black squares) of SO coupling. Panel B: DQD effective g^* factor as function of magnetic field and interdot barrier; g^* is calculated from spin expectation value difference between the two lowest levels, in units of g_0.

the states, as the magnetic field ↑ polarizes the low-energy states in the high-B limit (which eventually results in the formation of spin-polarized Landau levels). For a given V_b, the high gradient region in g^* occurs for field values near the anticrossing field, where the spin inversion takes place. One important feature, a change in the sign of g^*, is visible at high V_b and small field; notice that the field range in which the sign remains negative increases with interdot barrier (compare plots for $V_b=25$, 30, and 35 meV). Such a change in sign, impossible in the absence of SO couplings, is due to the delicate interplay of the magnetic, SO, and tunneling energies, for the nearly-degenerate two lowest DQD levels at high V_b. As such, one could also predict that the spin relaxation among them would exhibit distinct and nonmonotonic features, with possible minima and maxima as verified in the single-dot case.[11]

To further understand SO coupling on the DQD one-electron spectrum, we study the spin properties of the low-energy levels in Fig. 3. The left panels present the spin expectation value $\langle\sigma_z\rangle$ of each state as function of B for three distinct barriers; they show how the anticrossing between the two lowest excited states, at $B_{c,1e}$, moves toward smaller B fields with increasing V_b. The spin mixing is stronger near zero field as the barrier increases due to the dominance of SO over Zeeman terms. Notice also the competing roles of electron tunneling and magnetic field: in the strong-coupling regime [smaller V_b and larger $\delta(B=0)$], a higher value of $B_{c,1e}$ is needed to achieve the polarization of the two lowest levels, requiring a stronger Zeeman effect to overcome the large

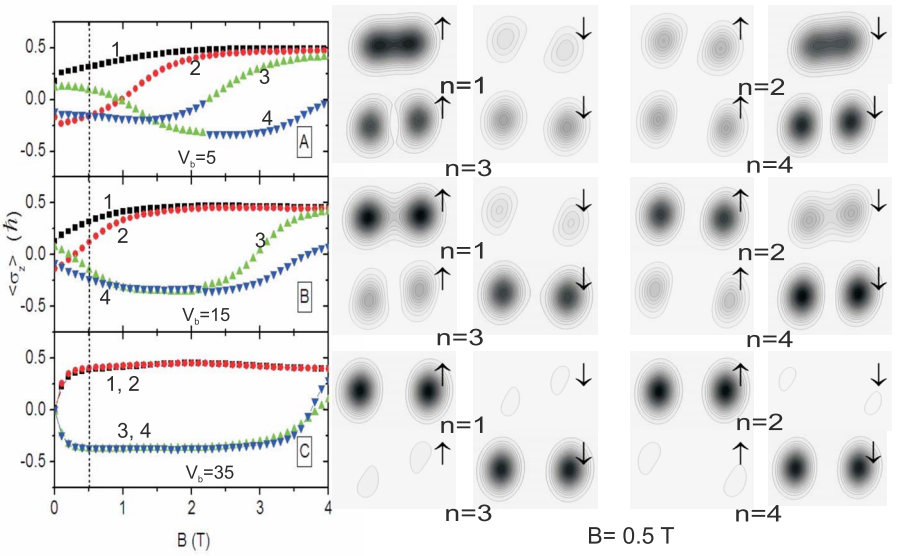

FIG. 3. (Color online) Left panels: single-electron spin expectation value $\langle\sigma_z\rangle$ as function of magnetic field. Panels A, B, and C refer, respectively, to V_b=5, 15, and 35 meV; vertical dashed line indicates B=0.5 T. Black squares, red circles, green up triangles, and blue down triangles indicate lowest levels n=1, 2, 3, and 4, respectively. Right panels: spin-density maps at B=0.5 T of the four lowest levels for the barriers on left panels.

interdot hopping integral $\delta(B=0)$. In the opposite regime, such polarization occurs even close to the zero-field limit, as $\delta \simeq 0$. At higher magnetic fields ($B>4$ T, not shown), the four lowest states become ↑ polarized ($\langle\sigma_z\rangle \simeq 1/2$) into the lowest Landau level, where SO coupling is dominated by magnetic terms.

The majority-spin component of the levels is clearly affected by SO. For example, at $B=0$, the states $n=1$ (ground state) and $n=3$ ($n=2$ and $n=4$) are predominantly ↑ (↓) in panel A; the spin majority is less obvious in panel B, as $|\langle\sigma_z\rangle| \ll 1/2$ for all levels, and in panel C the mixing is so strong that the four s states show $\langle\sigma_z\rangle \simeq 0$. Notice in panel C that a small B field is needed to differentiate between the levels, and the states $n=1$ and 2 ($n=3$ and 4) become ↑ (↓) rapidly, at $B \gtrsim 0.5$ T.

The right panels in Fig. 3 show the corresponding spin-density maps of the four lowest levels at $B=0.5$ T. One confirms that levels 1 and 3 (2 and 4) have majority ↑ (↓) at $V_b=5$ meV, where $B<B_{c,1e} \simeq 1$ T, but $n=2$, 3 and 4 have significant amplitude in both spin components. For $V_b=15$ meV, where $B>B_{c,1e} \simeq 0.3$ T, states 2 and 3 reverse their majority spin, and at $V_b=35$ meV states 1 and 2 (3 and 4) are almost purely ↑ (↓). These panels also clearly show that, as expected, increasing the barrier decreases the amplitude in the interdot region of the ground state, reducing $\delta(B=0)$ and the covalent character of the DQD ground state.

IV. TWO-ELECTRON LEVEL STRUCTURE

Figure 4 shows the two-electron spectrum for strong ($V_b=5$ meV, panel A) and weak ($V_b=35$ meV, panel B) interdot coupling regimes. Starting again from the spectra without SO coupling (blue dashed lines), panel A presents the usual splitting under B field of the T_+, T_- components of the (lowest) triplet, while the lowest energy singlet S only displays a diamagnetic shift. In contrast, panel B shows that, as a consequence of the vanishing electron tunneling at high V_b, states S and T_0 remain essentially degenerate at every B field, and the singlet is no longer the ground state. Accordingly, at $B \simeq 0$, the ground-state character changes from S (at $\simeq$17 meV in panel A) to T_+ (at $\simeq$29 meV in panel B). In panel A, the lowest S-T_+ crossing occurs at $B_{c,2e} \simeq 0.4$ T, and the zero-field S-T energy splitting is $\Delta(B=0) \simeq 1.5$ meV. The twofold degeneracy without SO coupling, indicated in several levels of Fig. 4(B), involves states S and T_0 (or two excited S states) at 28 (or 33) meV, and remains at finite field since it is due to the vanishing electron tunneling at high V_b. At zero field, the DQD ground state contains one electron per dot but with *opposite* spins, an S state; the value of $B_{c,2e}$ indicates the field needed to *flip* the spin of one of the

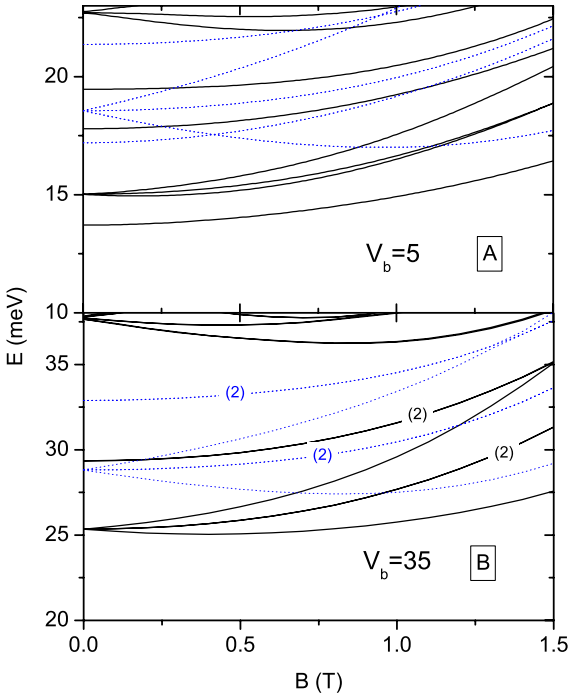

FIG. 4. (Color online) Two-electron level structure as function of magnetic field. Panels A and B refer to V_b=5 and 35 meV, respectively. Black solid (blue dashed) lines show spectrum with (without) SO coupling. Level degeneracies are indicated in parenthesis in panel B.

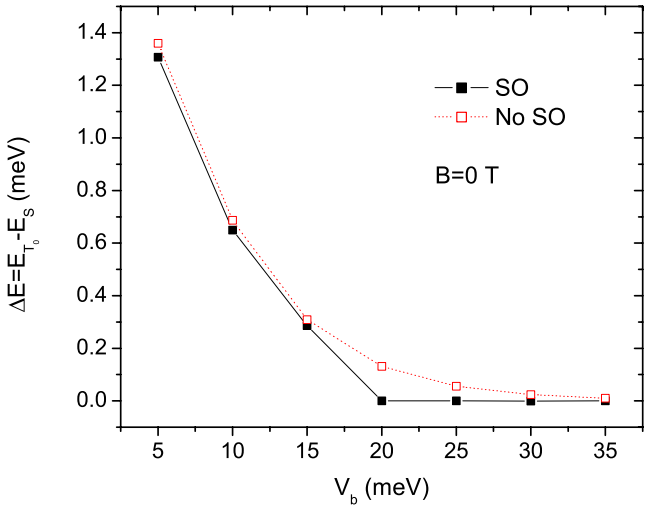

FIG. 5. (Color online) Effective exchange energy as function of barrier parameter value, $\Delta E = E_{T_0} - E_S$, for $B=0$ in the DQD system. Solid line and symbols include SO interactions.

electrons. Excited configurations with two electrons in either the right or the left dot are also present in the spectra, such as the second twofold degenerate set in panel B ($\simeq 33$ meV at $B=0$), corresponding to the two excited S states with double electron occupancy in either the right or left dot.

Like in the one-electron case, as the barrier increases (panel B), the spectrum is shifted upward, while $B_{c,2e}$ and $\Delta(B=0)$ decrease. Therefore, while in an isolated dot—and in a strongly coupled DQD—a finite B field is needed to achieve a S-T_+ transition, in a weakly coupled DQD such a degeneracy is already present at $B \simeq 0$.

The inclusion of SO coupling in Fig. 4 (black solid lines), as in the one-electron case, shifts the spectra downward and turns the crossing at $B_{c,2e}$ into an anticrossing, while the value of $\Delta(B=0)$ is nearly unaffected (see below). Despite changing the level dispersions significantly, especially at small fields where it dominates (notice that the first two excited states become almost degenerate in panel A), the SO coupling does not remove the twofold degeneracies in panel B produced by the left-right symmetry of the nearly uncoupled dots at that V_b value. Notice also that SO coupling dominates at low fields, resulting in smaller Zeeman splitting (smaller g^* factor) of the low-energy triplet. Indeed, the spin $\langle S_z \rangle$ expectation values would be expected to deviate from the pure 0, ± 1 values due to such strong SO influence in narrow-gap materials, as we find to be the case.

The singlet-triplet energy difference in the DQD system also is affected by the presence of SO coupling. Figure 5 shows this exchange energy with and without SO interactions. Although the spin character of the low-energy states is mixed in the presence of SO, we can obtain the energy difference between the nondegenerate S-like state and the nearby triplet manifold (degenerate at $B=0$) associated with T_0. This exchange energy difference is only slightly suppressed in the presence of SO coupling, except for $V_b \simeq 20$ meV, where the SO interaction results in the near fourfold degeneracy of the singlet-triplet set.

To study the spin properties in more detail, Fig. 6 shows

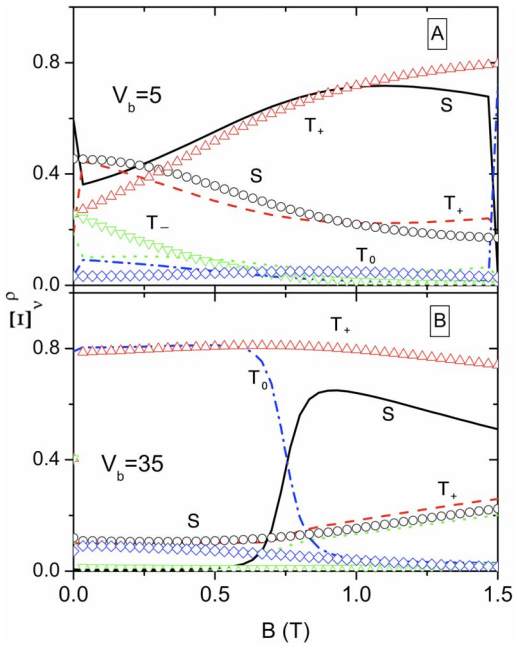

FIG. 6. (Color online) Spin probabilities of ground (symbols) and first excited (lines) DQD states for $V_b=5$ (panel A) and 35 meV (panel B). Black circles (solid line) indicate singlet component ($\rho = S$); red up triangles (dashed line) for T_+ component; green down triangles (dotted line) for T_-; blue diamonds (dash-dotted line) for T_0. Few curves have explicit labels.

$\Xi_\nu^\rho = \Sigma_{jk} |C_{j,k}^{\nu,\rho}|^2$ for a given spin ρ, for both ground ($\nu=1$) and first excited ($\nu=2$) states, in the strong (panel A) and weak (panel B) coupling regimes. The ground-state spin components (symbols) in panel A show it is clearly a mixture of S, T_+, T_- at $B=0$, but it becomes predominantly T_+ well after $B \simeq 0.5$ T. On the other hand, the ground state in panel B is predominantly T_+ right from $B \simeq 0$, acquiring a small S component at higher magnetic fields. As for the first-excited state (lines) in panel A, it is seen also to be a mixture of S, T_+, T_- at $B=0$, becoming predominantly S just after 0.5 T until 1.5 T, when it crosses with the next excited state which is mostly T_0 [check Fig. 4(A)]. The first-excited state in panel B, on the other hand, shows an interesting feature: despite the S-T_0 near degeneracy at any magnetic field [check Fig. 4(B)], there is a slight energy splitting so that this state is mostly T_0 until $\simeq 0.75$ T when it becomes mostly S, while at higher fields both the T_+ and T_- components increase at the expense of S.

V. CONCLUSION

We have shown that the strong influence of SO coupling in narrow-gap materials introduces a rich interplay with other energy scales in the system, namely, tunneling, magnetic, and exchange energies. This results in strong effects on the spectral properties of the double dot system and in highly structured spin textures for the lowest states. In particular, the singlet-triplet subspace [and its (anti) crossings] exhibits a much more involved behavior with magnetic fields, which affects the properties needed for definition and operation of spin qubit gates.

Although the results presented here are for a specific DQD structure, the behavior is in fact generic. Notice that while we have studied in detail the variation in the interdot barrier, qualitatively similar results are expected for fixed structure geometry but different interdot distances.

As such, the sizeable level anticrossings and accompanying spin mixtures, as well as smaller g^* factors, will be common in narrow gap materials and should be carefully taken into account when considering the use of these states as part of basic qubit states. The characteristic energy (or time) scales are comparable to some of those in single quantum dots, and would likely give rise to interesting behavior in the phonon-assisted spin-relaxation rates. Theoretical investigation of these rates is under consideration and will be presented elsewhere.

ACKNOWLEDGMENTS

We acknowledge support from NSF Grants No. 0336431 and No. 0710581, CONACyT-Mexico 36764, and the Glidden VP and CMSS Programs at Ohio University.

[1] D. Loss and D. P. DiVincenzo, Phys. Rev. A **57**, 120 (1998).
[2] F. H. L. Koppens, C. Buizert, K. J. Tielrooij, I. T. Vink, K. C. Nowack, T. Meunier, L. P. Kouwenhoven, and L. M. K. Vandersypen, Nature (London) **442**, 766 (2006).
[3] J. R. Petta, A. C. Johnson, J. M. Taylor, E. A. Laird, A. Yacoby, M. D. Lukin, C. M. Marcus, M. P. Hanson, and A. C. Gossard, Science **309**, 2180 (2005).
[4] K. M. Svore, D. P. DiVincenzo, and B. M. Terhal, Quantum Inf. Comput. **7**, 297 (2007).
[5] I. A. Merkulov, A. L. Efros, and M. Rosen, Phys. Rev. B **65**, 205309 (2002).
[6] A. V. Khaetskii, D. Loss, and L. Glazman, Phys. Rev. Lett. **88**, 186802 (2002).
[7] J. M. Elzerman, R. Hanson, L. H. W. van Beveren, B. Witkamp, L. M. K. Vandersypen, and L. P. Kouwenhoven, Nature (London) **430**, 431 (2004).
[8] S. Amasha, K. MacLean, I. P. Radu, D. M. Zumbuhl, M. A. Kastner, M. P. Hanson, and A. C. Gossard, Phys. Rev. Lett. **100**, 046803 (2008).
[9] A. V. Khaetskii and Y. V. Nazarov, Phys. Rev. B **61**, 12639 (2000); **64**, 125316 (2001).
[10] V. N. Golovach, A. Khaetskii, and D. Loss, Phys. Rev. Lett. **93**, 016601 (2004).
[11] C. F. Destefani and S. E. Ulloa, Phys. Rev. B **72**, 115326 (2005).
[12] P. Stano and J. Fabian, Phys. Rev. Lett. **96**, 186602 (2006).
[13] L. Meier, G. Salis, I. Shorubalko, E. Gini, S. Schon, and K. Ensslin, Nat. Phys. **3**, 650 (2007).
[14] Y. A. Bychkov and E. I. Rashba, J. Phys. C **17**, 6039 (1984).
[15] G. Dresselhaus, Phys. Rev. **100**, 580 (1955).
[16] P. Stano and J. Fabian, Phys. Rev. B **72**, 155410 (2005).
[17] J. Konemann, R. J. Haug, D. K. Maude, V. I. Fal'ko, and B. L. Altshuler, Phys. Rev. Lett. **94**, 226404 (2005).
[18] G. Burkard, D. Loss, and D. P. DiVincenzo, Phys. Rev. B **59**, 2070 (1999).
[19] G. Burkard and D. Loss, Phys. Rev. Lett. **88**, 047903 (2002).
[20] D. Stepanenko, N. E. Bonesteel, D. P. DiVincenzo, G. Burkard, and D. Loss, Phys. Rev. B **68**, 115306 (2003).
[21] M. Florescu and P. Hawrylak, Phys. Rev. B **73**, 045304 (2006).
[22] A. Bagga, P. Pietilainen, and T. Chakraborty, Phys. Rev. B **74**, 033313 (2006).
[23] C. F. Destefani, S. E. Ulloa, and G. E. Marques, Phys. Rev. B **69**, 125302 (2004); **70**, 205315 (2004).
[24] X. Hu and S. Das Sarma, Phys. Rev. A **61**, 062301 (2000).
[25] Parameters used are $V_r = V_l = 50$ meV, $a = 40$, $l_r = l_l = 50$, $l_{bx} = 25$, $l_{by} = 50$, and $z_0 = 4$, lengths in nm. Also, $dV/dz = -5$ meV/nm, $g_0 = -51$, $\varepsilon = 16.5$, $\alpha = 5$ nm^2, $m^* = 0.014$, and $\gamma = 160$ meV/nm^3. Convergence is carefully monitored; the grid size is typically well over 20,000, and we use over ten one-particle basis sets.
[26] C. F. Destefani and S. E. Ulloa, Phys. Rev. B **71**, 161303(R) (2005).